RE-TRANSPORT MECHANISMS OF FALLEN POLLEN BY SURFACE-CREEP AND SALTATION

ICHIRO NAKANE

Department of Mechanical Engineering, Kanagawa Institute of Technology, Atsugi 243-0292, Japan
E-mail: inakane@me.kanagawa-it.ac.jp

Abstract- The cedar pollinosis is a very serious problem in Japan. The prevalence of this pollinosis is considered more than 20% among the Japanese. In the point of avoiding pollen exposure, it is important to clarify the pollen transport mechanisms. In particular, in urban areas of Japan, the house has been built to be nearly in contact with another. If the fallen pollen on the roof is re-transported and falls down to the lower level, the exposure amount will increase drastically. Accordingly, in this study, we focus on the re-transport mechanisms of the fallen pollen on surfaces and carried out the wind tunnel experiments by using test particles to clarify the pollen exposure from roofs. The test particles are carried by the wind, and move (creep) along or jump (saltate) repeatedly on the surface. Consequently, we discuss the followings in this paper: the optical measurement of surface-creep and saltation behavior of the test particles, the generality of the flow field in this study and the possible conditions of re-transport from a surface.

Keywords- Flow Visualization, Multi-phase Flow, Particle Tracking Velocimetry, Pollen Transportation

I. INTRODUCTION

The number of people suffering from Japanese cedar (Cryptomeria japonica) pollinosis continues to grow. In particular, in the Tokyo metropolitan area, a survey reports that the increase in the rate of occurrence between the ages of 0 and 14 years is extremely high by more than 10 times in the last 20 years [1]. The increase in the rate of occurrence of Japanese cedar pollinosis among young people born and raised in Tokyo simply means an increase in pollen exposure in Tokyo, and it is considered as a major problem that must be alleviated.

The pollen of Japanese cedar is carried by the wind, but its aerodynamic diameter d_a is comparatively large, d_a=35μm. Consequently, the pollen falls to the surface in light winds, which differentiates it from Suspended Particulate Matter. This is the reason why cedar pollen is dispersed over distances of only several tens of kilometers. However, according to Pye [2], strong winds can resuspend (or redisperse) particles such as the pollen from surfaces at low heights and over short distances, and this phenomenon may increase the pollen exposure levels. In particular, in urban areas of Japan, the house has been built to be nearly in contact with another as shown in Fig. 1. If the pollen on roofs is re-transported and falls down to the lower level, the pollen exposure amount will increase drastically.

In fact, we measured the atmospheric pollen in the valley of the building during the pollen scattering season (last spring). The amount of pollen at the same level as the nearest building roof is about 1.4 times larger than that of higher place and about 2.6 times larger than that of lower place. However, we can't judge that the increased amount of pollen is influenced only by resuspending from the roof, because the wind velocity is also fastest at the height of the largest amount of pollen.



Imagery ©2015 TerraMetrics, Map data ©2015Google, Zenrin

Fig.1 An example of Tokyo residential area

In this study, we aim to clarify the re-transport influence from roofs on the total pollen exposure. We carried out the wind tunnel experiments with using test particles to study the re-transport mechanisms of fallen pollen by surface-creep and saltation.

II. PARTICLE SURFACE-CREEP AND SALTATION BEHAVIOR IN A FLAT PLATE BOUNDARY LAYER

A. Test Particle Substituted for Japanese Cedar Pollen

The aerodynamic diameter of Japanese cedar pollen is measured as about d_{am}=35μm [3]. With substituting for Japanese cedar pollen, we selected the test particle that has approximately the same aerodynamic diameter of this pollen, because this pollen causes the allergic serious damage to our nose and eyes.

After all, I use Lycopodium clavatum spore as the test particle, because this spore causes almost no damage to us and the mean aerodynamic diameter d_{am}=33μm is nearly the same as Japanese cedar pollen [3]. Lycopodium clavatum spore is provided as a standard powder by the Association of Powder Process Industry & Engineering, Japan (APPIE), and the distribution of

particle diameters, particle density, etc., is given explicitly for each batch. Other advantages of using this spore include the fact that it does not absorb moisture, is not self-adherent, and has excellent fluidity. The characteristics of this spore are shown in Table 1.

Table 1 The characteristics of the test particle
(Test particle: Lycopodium clavatum spore)

Diameter d	from 20μm to 50μm
Mean Diameter d_m	32 [μm]
Terminal velocity by Stokes' Law V_t	32.5 [mm/s]
Aerodynamic Diameter d_a	33 [μm]
Particle Density ρ_p	1.05 [g/cm^3]

Here, restricting to just anemophilous plants, the range of densities of pollen species is 0.39–1.1 g/cm^3, and the range of densities of spore species is 0.56–1.44 g/cm^3. Furthermore, these particle diameters, regardless of the pollen or spore species, are approximately 50 μm or less. The density and diameter of Lycopodium clavatum spore, therefore, represent intermediate values for the pollen and spore species, and thus the findings of this study are anticipated to be equally applicable for many pollen and spore species. To elucidate both the shape and size of Lycopodium clavatum spore and Japanese cedar pollen, micrographs of each are shown in Fig. 2 and 3, respectively.

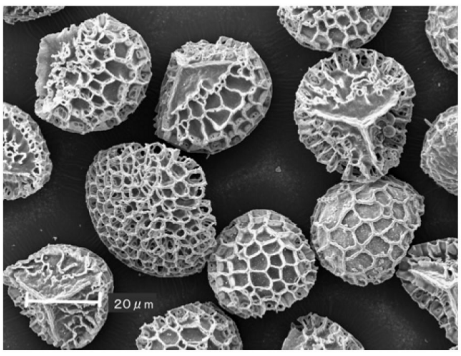


Fig.2 Electron microscope image of Lycopodium clavatum spores (Test particle) (Copyright permission from The Association of Powder Process Industry and Engineering, JAPAN)

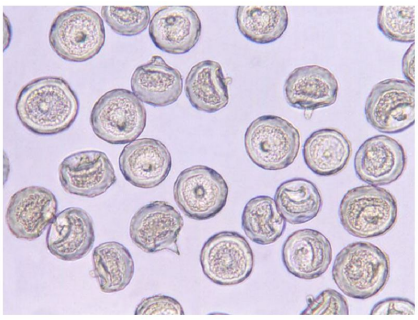


Fig.3 Optical microscope images of Japanese cedar pollen
(Copyright permission from JST: Rika-network)

B. Experimental Apparatus to Observe and Measure the Test Particle Behavior

We observed and measured the surface-creep and saltation behavior of the test particle using a high speed video camera and PTV method. The schematic diagram of experimental apparatus is shown in Fig.4. Fig.4 shows that the flat steel plate that is grounded to prevent adhesion by static electricity is set up in the recirculating wind tunnel and the test particles are scattered on this plate. These particles are irradiated with the green laser light sheet, and the transport behavior of them is recorded by a high speed video camera. The velocities of the test particles are obtained by PTV method, and the main stream velocity U and the boundary layer velocity u (y=2.5mm) are measured by hot wire anemometers. Furthermore, the shutter is attached to the wind tunnel outlet and opens much quickly by the gravity.

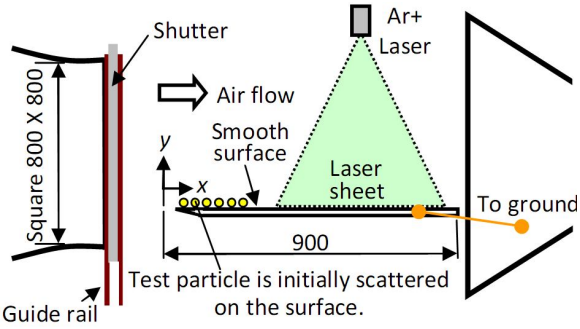


Fig.4 Schematic diagram of experimental apparatus to observe and measure the test particle transfer behavior

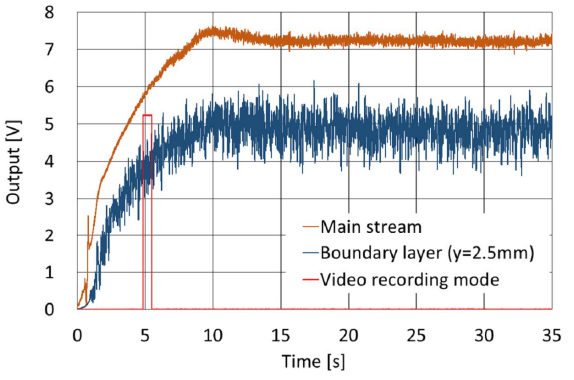


Fig.5 An example of the time sequential output voltage of the hot wire anemometers and high speed video camera in the case of U=5m/s and t_s=4.82s

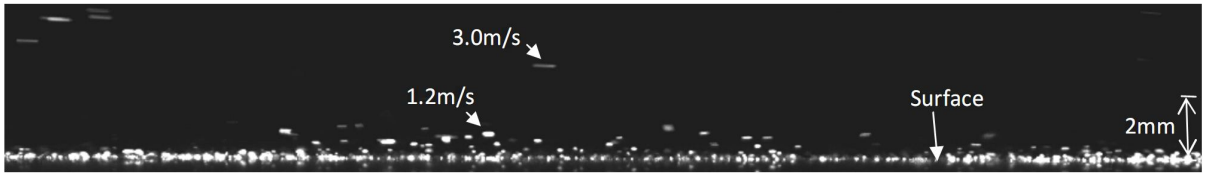
The observation and measurement begin with opening the shutter and air simultaneously blows out at the defined velocity. Fig.5 shows an example of the time sequential output voltage of the hot wire anemometers and high speed video camera in the condition of U=5m/s. The main stream and boundary layer velocities are obtained by multiplying 0.7 to the output voltage of the anemometers. The high speed video camera outputs TTL level voltage (5V) in the recording mode. From opening the shutter, the boundary layer velocity u fluctuates largely about 1s

later, the main stream velocity U becomes constant at the defined velocity about 15s later, and the ratio of boundary layer velocity to main stream velocity u/U becomes constant about 3s later. When we observed the test particle transport behavior, we changed the main stream velocity (U=3m/s, U=5m/s, U=10m/s) and the recording start time t_s of the high speed video camera. In addition, t_s. is changed variously, but the recording time of the high speed video camera is constant (0.68s).

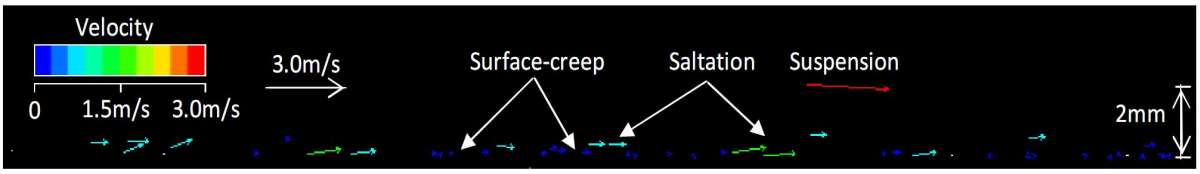
C. Observed and Measured the Surface-creep and Saltation Behavior of the Test Particle

Some examples of the results obtained by the high speed video camera are shown in the following. Fig.6 shows an image recorded at 6000fps in Fig.(a) and the test particle velocity distribution obtained by PTV measurement in Fig.(b). Furthermore, the time sequential main stream and boundary layer velocity profiles synchronized with these results of Fig.6 are shown in Fig.7. In Fig.6(a), we can see that the fast particles are multiple exposure even in 6000fps. Consequently, we can calculate the velocity of the fast particle by the path line image, and we really calculated two points. This result is valid by inferring from the boundary layer velocity in Fig.7, and we may calculate the fast particle velocity without raising the frame rate. However, we can't apply this path line method under the mix of slow and fast particles, and we used PTV method. Fig.6(b) shows that the test particles are being transported with various forms. These velocities are also valid by inferring from the velocity in Fig.6(a) and 7. In particular, the velocities of the surface-creep particles are much slower than the saltation and suspension particles. Their velocities are less than about 0.1m/s.

Fig.6 shows that many particles are transported with the surface-creep and saltation but a few particles are suspended. The typical process until suspension is shown as Fig.8. Fig.8 shows the time sequential pictures of the collision between the high and low velocity particles. In the moment of collision, one jumps upward at high velocity and reaches the suspension. However, in this case, the high velocity particle is saltating before collision. By jumping upward, the particle resultant velocity increases by the faster carrier air flow, even if this jump is a little. By repeating the collision and jumping, the particle increases its velocity and reaches enough height.



(a) An image recorded at 6000fps by the high speed video camera (U=5m/s, t=5.17s)



(b) Test particle velocity distribution obtained by PTV measurement (U=5m/s, t=5.14s)

Fig.6 The results obtained by the high speed video camera

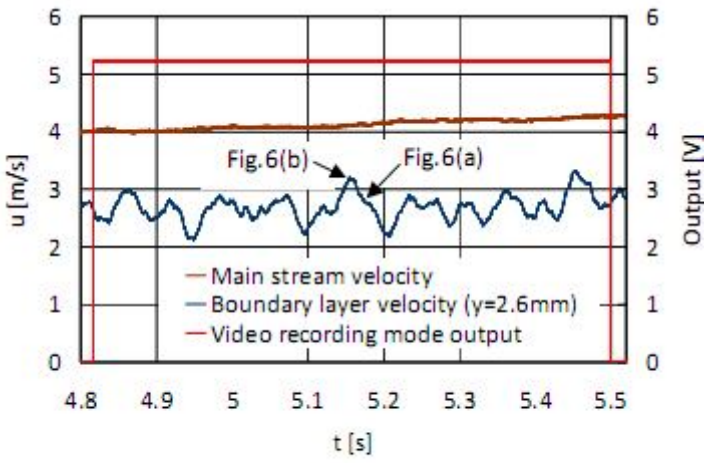


Fig.7 The time sequential main stream and boundary layer velocity profiles synchronized with Fig.6

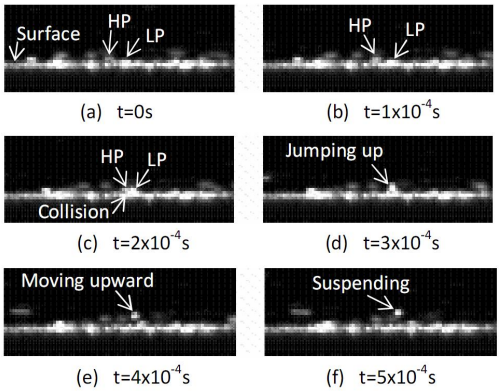


Fig.8 Typical sequential process until suspension by the high speed video camera at 10000fps (U=10m/s)
(HP : High velocity particle, LP : Low velocity particle)

We can't show all results in detail, and thus the particle transport behavior is summarized in table 2. Now, it is important that the test particles are almost still and aren't transported in the condition of U=3m/s.

Table 2 The transport behavior of the test particle

Transport type	Stillness	Surface-creep	Saltation
U=3m/s	◎	△	×
U=5m/s	○	○	○
U=10m/s	△	△	◎

◎: Almost , ○: Frequently , △: Sometimes , ×: Rarely

III. BOUNDARY LAYER VELOCITY MEASUREMENT

In the previous chapter, we discussed the transport behavior of the test particle that was carried by the air flow. Accordingly, we also try to clarify the characteristics and to confirm the generality of the flow field. The boundary layer velocity is measured by traversing the hot-wire probe. This result is shown in Fig.9. In Fig.9, □ is a boundary layer thickness, u' is turbulent fluctuation velocity and the overbar means time-mean value. Fig.(a) shows the time-mean velocity and Fig.(b) shows the autocorrelation of the fluctuating velocity. We consider only the time-mean value of the boundary layer velocity in this chapter, but we show the behavior in the unsteady conditions in the previous chapter. However, in oscillating turbulent flow, the near-wall velocity is known to change while maintaining the similarity relationship [4]. Consequently, we think that the flow field velocity shown as the previous chapter is being accelerated while maintaining the similar velocity profiles of the steady state shown as this chapter. In fact, in the previous chapter, we show that the ratio of boundary layer velocity to main stream velocity u/U is almost constant.

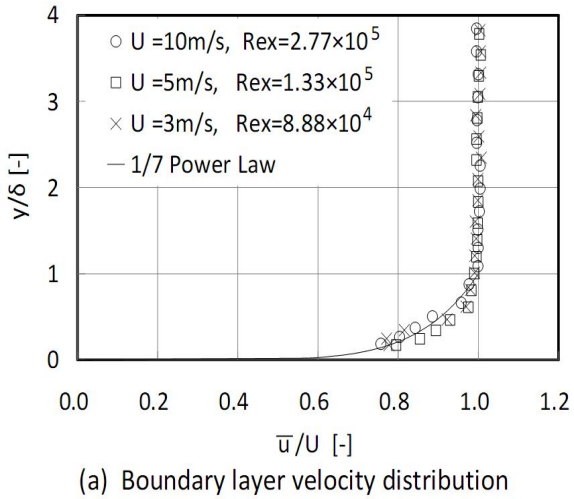
Fig.9 shows little difference due to the Reynolds number Re_x. In particular, the boundary layer velocity profile is almost same as the 1/7 Power Law (the seventh root profile) which is valid for the Reynolds number range of $10^5 < Re_x < 10^6$. The value and profile of the turbulent intensity is also common. Therefore, we think that the flow transporting the test particles in this study has high generality and the results obtained by this study can apply generally. Here, we calculate the friction velocity u_τ for further consideration. We used the Clauser chart method and this chart is shown as Fig.10. The details of this method, for example, may refer to Wei et al [5]. That is, there is the relation of the following equation (1) between the gradient of this chart and the friction velocity u_τ.

$$Gradient = \frac{u_\tau}{\kappa U} \qquad \kappa\ (\text{Karman constant}) = 0.41 \tag{1}$$

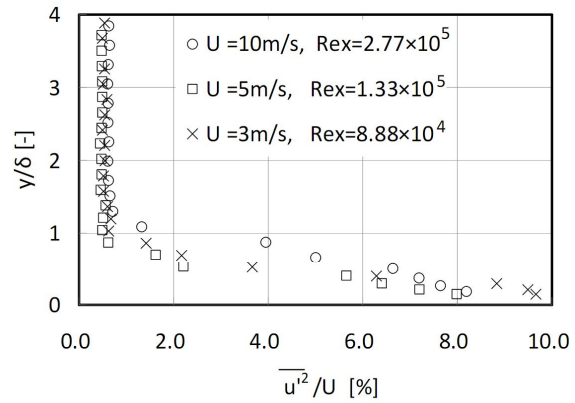
The calculated friction velocities are summarized in Table 3. The upper u_τ is calculated by this Clauser chart method (Eq.(1)) and the lower u_τ is calculated by the next equation (2) that is based on the seventh root profile.

$$C_f = \frac{0.027}{\mathrm{Re}_x^{1/7}} \qquad u_\tau = \sqrt{\frac{C_f}{2}}U \tag{2}$$

The difference between the upper and lower value is less than about 10% and the generality of the flow is also confirmed by u_τ.



(a) Boundary layer velocity distribution



(b) Turbulent intensity distribution

Fig.9 Measured mean and fluctuation velocity distribution in the boundary layer on the flat plate

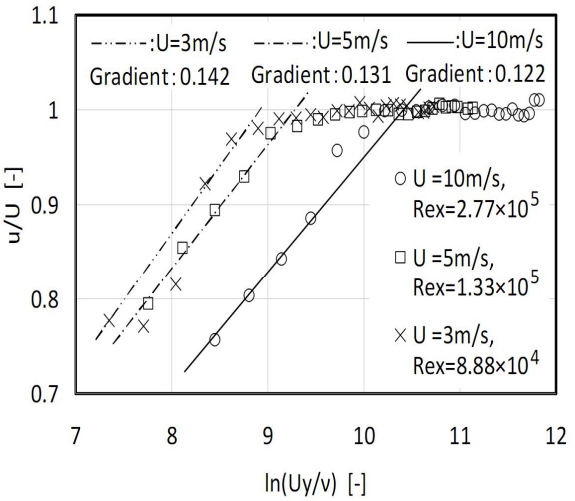


Fig.10 Clauser chart

Table 3 The calculated friction velocity

Re_x	8.88 X 10^4	1.33 X 10^5	2.77 X 10^5
u_t : Eq.(1)	0.194m/s	0.268m/s	0.519m/s
u_t : Eq.(2)	0.172m/s	0.250m/s	0.493m/s

IV. THE CONDITIONS OF POSSIBILITY OF RE-TRANSPORT OF FALLEN POLLEN ON SURFACE

We consider the conditions of possibility of re-transport of fallen pollen, because it is serious problem for pollen exposure whether the fallen pollen on roofs can be transported or not. For example, in this previous chapter, we show that the test particles keep still in the weak main stream U=3m/s.

If the fallen pollen on roofs also keeps still, pollen exposure will be reduced. We consider the balance of forces on the stationary test particle. It becomes Fig.11 by illustrating the forces.

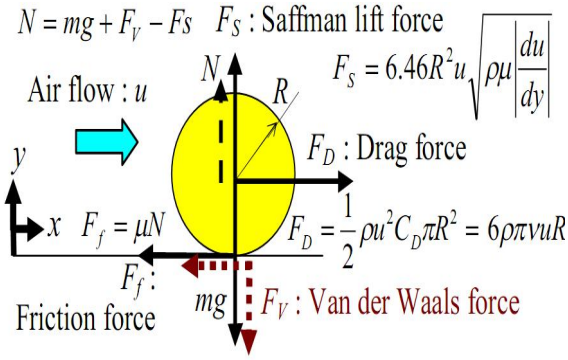


Fig.11 Balance of forces on the stationary test particle

Van der Waals force F_V is isotropic and we assume that F_V acts equally in the x- and y-directions.

When the test particle keeps still in the flow field, we acquire the following condition (equation).

$$\mu N > F_D - F_V \qquad (3)$$

Here, it is assumed that various adhesion forces are included to F_V, because van der Waals force is largest in the adhesion forces [6]. Now, we need to estimate van der Waals force F_V. However, it is too difficult to determine F_V, because van der Waals force is greatly affected by the contact surface.

Accordingly, we repeated the experiment by using an inclined plane and assume that van der Waals force is almost equal to gravity.

In general, van der Waals force becomes to be about a hundred times of gravity, but Lycopodium clavatum spore (test particle) has low adhesion property, thus we assume the hypothesis $F_V = mg$ in this paper.

The test particles accumulate in contact with the surface. They are in the viscous sublayer, and the velocity around them is the following.

$$\frac{u}{u_\tau} = \frac{u_\tau y}{\nu} \quad \therefore \quad u = \frac{u_\tau^2 R}{\nu} \quad \therefore \quad \frac{du}{dy} = \frac{u_\tau^2}{\nu} \qquad (4)$$

Consequently, Eq.(3) is as follows:

$$\mu > \frac{18\pi\rho\nu u_\tau^2 - 4\pi\rho_p \nu R g}{8\pi\rho_p \nu R g - 19.38\rho R u_\tau^3} \qquad (5)$$

In Eq.(5), □ and □p are the air and particle density, respectively. Therefore, static friction coefficient

□ which the test particle needs for keeping still is the function of friction velocity u□. This relationship between u□ and □ is shown in Fig.12.

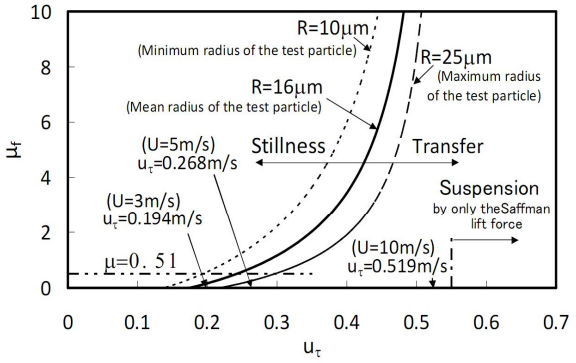


Fig.12 Static friction coefficient for the test particles to continue staying on the surface

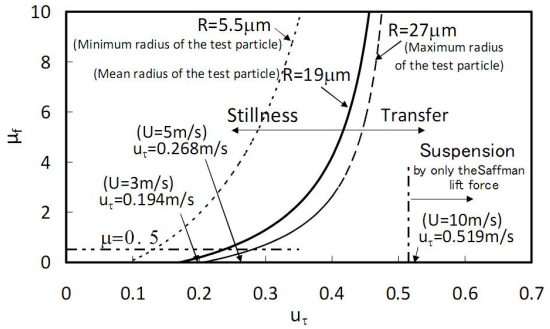


Fig.13 Static friction coefficient for Japanese cedar pollen to continue staying on the surface

Fig.12 shows that the smaller test particle is easily transported more than the larger one. For example, if the test particles don't transfer in the flow field of $u_{\square}$=0.3m/s, static friction coefficients of R=25□m and R=10□m become □ =0.53 and □ =2.22, respectively. It is easily understand that the small or light weight particle is transported by weak wind. Here, □ =0.51 in this figure shows the static friction coefficient of the test particle which was measured by using an inclined plane, and using this value, we discuss the consistency of the results of the previous chapters. In the case of □ =0.51, each particle doesn't transfer under the following conditions: R=10□m ; $u_{\square}$=0.195m/s, R=16□m ; $u_{\square}$=0.243m/s, R=25□m ; $u_{\square}$=0.297m/s.

Consequently, the following are predicted:
1) In the flow field of U=3m/s, all particles keep still.
2) In the flow field of U=5m/s, extremely large particles don't transfer but many particles are transported by the flow.
3) In the flow field of U=10m/s, all particles are transported by the flow.
The above predictions are well consistent with Table 2, and we predict the Japanese cedar pollen behavior with the same manner.

We show the result in the case of Japanese cedar pollen in Fig.13 with the same manner as Fig.12. The differences between Fig.12 and Fig.13 are less, because the aerodynamic diameter of the test particle is nearly equal to Japanese cedar pollen. However, the minimum radius of Japanese cedar pollen is much smaller than that of the test particle [3], thus this profile is only different.

In other words, in the case of Japanese cedar pollen, the extremely small pollen are only transported in the condition of U=3m/s.

The pollen with various size can be almost transported by the main stream velocity U=5m/s. However, since this knowledge is obtained from the experiments being carried on by the wind tunnel, it is necessary to further study in order to apply to the actual phenomena.

CONCLUSION

We considered re-transport mechanisms of fallen pollen, because we worry that the re-transport of pollen increases the amount of pollen exposure. We carried out the wind tunnel experiments and obtained the following results:
1) In the case of U=3m/s, almost all test particles keep still.
2) In the case of U=5m/s, all types of transport behavior of particles: surface-creep, saltation and suspension appear, and some test particles in contact with the surface don't move.
3) In the case of U=10m/s, many test particles saltate and are suspended, but few test particles in contact with the surface don't move.
4) Test particles jump higher by particle-wall and particle-particle collisions.
5) Regardless of the types of transport behavior, test particles transfer with the same velocity as the air flow.
Furthermore, we also studied the model to predict the types of transport behavior by friction velocity. The validity of this model was confirmed by the wind tunnel experiments. However, it is necessary to further study in order to apply this model to the actual phenomena.

REFERENCES

[1] Survey of Tokyo Metropolitan Government Bureau of Social Welfare and Public Health, “Pollinosis patient survey report (in Japanese)“, p. 17, 2007.
[2] K. Pye, “Aeolian dust and dust deposits”, Academic Press, p.49, 1987.
[3] I. Nakane, “Cedar Pollen Suspension and Saltation Transport Behavior (in Japanese)”, Transactions of the Japan Society of Mechanical Engineers Edition B, vol. 78, no. 790, pp. 1220-1234, 2012.
[4] S. Masuda and T. Muraishi, “A study of near-wall flow field of oscillating turbulent channel flow : 1st Report, Time mean and phase-averaged velocity (in Japanese)”, Transactions of the Japan Society of Mechanical Engineers Edition B, vol. 56, no. 523, pp. 628-635, 1990.
[5] T. Wei, R. Schmidt and P. McMurtry, “Comment on the Clauser chart method for determining the friction velocity”, Experiments in Fluids, vol. 38, pp. 695–699, 2005.
[6] H. Hasebe, Y. Yamada, Y. Suzuki, "Study on Reentrainment of Fine Particles Deposited on Duct Walls by Airflow (in Japanese)", Earozoru Kenkyu, Vol.29, No.3, pp. 190-195, 2014